Received: 14 September 2021 | Revised: 4 May 2022 | Accepted: 18 July 2022

DOI: 10.1002/mma.8621

RESEARCH ARTICLE

WILEY

Electromagnetic fields simulating a rotating sphere and its exterior with implications to the modeling of the heliosphere

Lorella Fatone[1] | **Daniele Funaro**[2]

[1]Dipartimento di Matematica, Università di Camerino, Camerino, Italy

[2]Dipartimento di Scienze Chimiche e Geologiche, Università di Modena e Reggio Emilia, Modena, Italy

Correspondence
Lorella Fatone, Dipartimento di Matematica, Università di Camerino, Via Madonna delle Carceri 9, 62032 Camerino, Italy.
Email: lorella.fatone@unicam.it

Communicated by: V. Kravchenko

Vector displacements expressed in spherical coordinates are proposed. They correspond to electromagnetic fields in vacuum that globally rotate about an axis and display many circular patterns on the surface of a ball. The fields satisfy the set of Maxwell's equations, and some connections with magnetohydrodynamics can also be established. The solutions are extended with continuity outside the ball. In order to avoid peripheral velocities of arbitrary magnitude, as it may happen for a rigid rotating body, they are organized to form successive encapsulated shells, with substructures recalling ball-bearing assemblies. A recipe for the construction of these solutions is provided by playing with the eigenfunctions of the vector Laplace operator. Some applications relative to astronomy are finally discussed.

KEYWORDS

associated Legendre polynomials, Bessel functions, eigenfunctions, electrodynamics, exact solutions

MSC CLASSIFICATION

33C47, 35Q61, 78A25

1 | FOREWORDS

The main practical achievement of this paper is the introduction of some exact solutions in the whole tridimensional space for a set of equations modeling electrodynamics. The result has by itself a general validity and can be applied in many circumstances emerging in the context of fluid dynamics, electromagnetism (EM), magnetohydrodynamics (MHD), or geophysics. It may also represent a referring point to develop numerical type simulations, especially in the context of spectral type approximation methods.

The fields are described in spherical coordinates and solve the whole set of Maxwell's equations in vacuum. They are spherical eigenfunctions of the vector Laplace operator, obtained by separation of variables. As usual, this procedure leads to trigonometric functions for the azimuthal angle and Bessel's functions for the radial component. As far as the altitude angle is concerned, one obtains a family of special functions that can be put in connection with the so-called associated Legendre polynomials (see Abramowitz and Stegun[1]). The displacement rigidly rotates about an axis at speeds comparable to that of light, with an angular velocity depending on a parameter ω. The setup of the equations and the structure of the solutions are given in Section 2. In Section 3, further properties are discussed.

We successively worked on the possibility to prolong the electromagnetic fields outside the ball. Since the above solutions are defined everywhere, a natural extension already exists. Nevertheless, such a straightforward expansion would bring to peripheral velocities of arbitrary magnitude, which is unphysical. The question is however well-posed, since the dynamical fields present on the ball surface may be used as boundary constraints to analyze the external problem. Such a study is partially approached in Landau and Lifschits,[2] section 89, from the relativistic viewpoint. Here, due to the lack of space, we will not touch on questions pertaining to the theory of relativity, although the argument is very appropriate. Some hints will be however given in Section 6.

It is important to remark that our problem is not directly related to the so-called lighthouse paradox, involving the dynamics of light rays escaping from a rotating source (see Figure 1). The difference is mainly due to the type of boundary conditions we are enforcing (radial in the lighthouse case, transverse in our case). Indeed, we would like to reproduce a situation where the rotating sphere is surrounded by another EM configuration evolving at lower angular velocity. The process may be repeated, so producing a sequence of encapsulated environments. The most important achievement is that the connections can be done by avoiding discontinuities. This brings us to the third picture of Figure 1, and to Figure 4. We postpone the discussion of the main idea to Section 4, by showing how this can be quantitatively implemented.

In Section 5, we add stationary fields to the dynamical solutions examined so far, and we examine the possible links with some model equations arising from the study of plasma. Section 7 is devoted to some considerations about the constitution of the Sun and the corresponding solar system that descend as a natural consequence of the analytic construction. Finally, in Section 8, we try to provide a possible justification of the Titus–Bode law, which rules the averaged distance of the planets from the Sun. Such a law is still in search of convincing theoretical explanations.

2 | PRELIMINARY SETTING

We start by introducing the classical Maxwell's equations in vacuum. We denote by **E** the electric field and by **B** the magnetic one. We first have the Ampère's law, with no current source term:

$$\frac{\partial \mathbf{E}}{\partial t} = c^2 \mathrm{curl}\mathbf{B}, \tag{1}$$

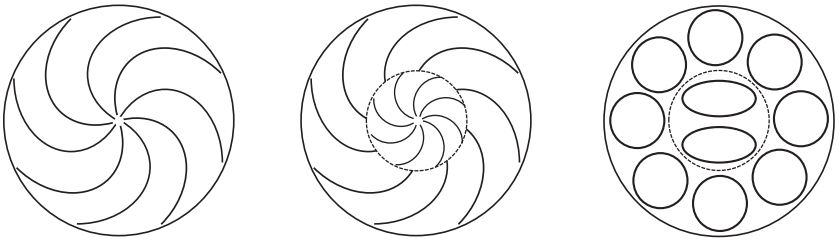

FIGURE 1 Due to the boundedness of the speed of light, as moving away from the central core, the spiraling patterns of the left picture, tend to break up after a certain time (central picture), unless suitable relativistic corrections are made. Due to the different type of boundary conditions, in our approach (right), a fast rotating core induces the rotation of an external one with a lower angular velocity. Differently from the previous case, this transfer can be done with continuity

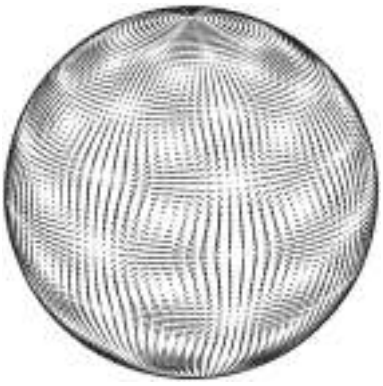

FIGURE 2 Electric field distribution on the surface of a ball having the radius corresponding to a zero of the function H. In this situation, the magnetic field is uniformly zero. The number of vortexes depends on the parameters. In the present case, we have $m = 4$ and $\ell = 11$

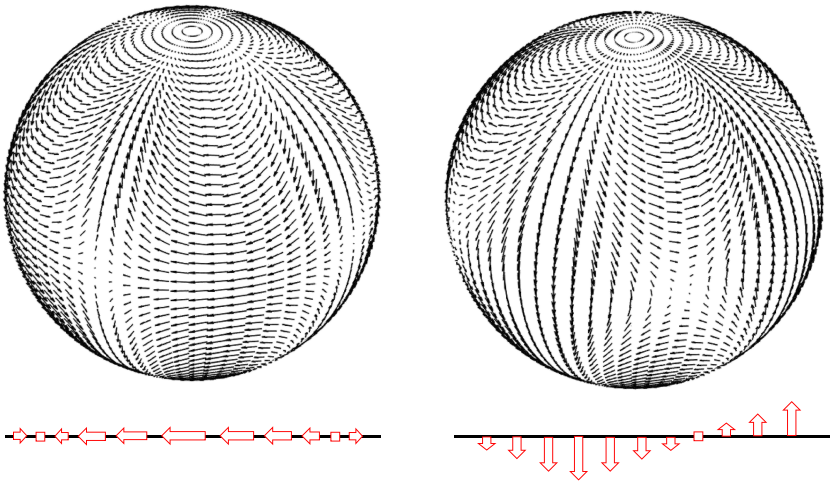

FIGURE 3 Field distributions: electric (left) for radial points where $H = 0$; magnetic (right) for radial points where $H \neq 0$. Both pictures refer to the situation $m = \ell = 2$. At the equator, the electric field oscillates horizontally, whereas the magnetic field is lined up with the meridians [Colour figure can be viewed at wileyonlinelibrary.com]

FIGURE 4 Ball-bearing assembly (left). In the referring frame where the spheres are at rest, the internal and the external boundaries counter rotate, displaying different angular velocities. A similar effect can be achieved by solving the wave equation in a suitable annular region (right). In this circumstance, the size and the frequencies involved must be wisely calibrated [Colour figure can be viewed at wileyonlinelibrary.com]

where c is the speed of light. Successively, we have the Faraday's law:

$$\frac{\partial \mathbf{B}}{\partial t} = -\mathrm{curl}\mathbf{E}. \tag{2}$$

Finally, we close the set with the following conditions on the divergence:

$$\mathrm{div}\mathbf{E} = 0, \tag{3}$$

$$\mathrm{div}\mathbf{B} = 0. \tag{4}$$

It is well known that, by suitably combining Equations (1)–(4), it is not difficult to arrive at the vector wave equations:

$$\frac{\partial^2 \mathbf{E}}{\partial t^2} = c^2\,\Delta\mathbf{E}, \qquad \frac{\partial^2 \mathbf{B}}{\partial t^2} = c^2\,\Delta\mathbf{B}. \tag{5}$$

We work in spherical coordinates (r, θ, ϕ). Hereafter, H will denote a function of the variable r, whereas S_2, S_3 will be functions of the variable $x = \cos\theta$. We also set $\zeta = c\omega t - m\phi$, where $\omega > 0$ is a parameter. This setting allows us to simulate the motion of an EM wave rotating around the vertical axis (orthogonal to the equatorial plane $\theta = \pi/2$). We then look for magnetic fields of the form:

$$\mathbf{B}_D = (B_r, B_\theta, B_\phi) = \frac{1}{c}\,(0,\, H(r)S_2(\cos\theta)\cos\zeta,\, H(r)S_3(\cos\theta)\sin\zeta)\,. \tag{6}$$

Thus, we have $B_r = 0$. The expression in (6) is required to satisfy the condition $\mathrm{div}\mathbf{B}_D = 0$ and the wave equation in (5). Going through classical computations, it is possible to achieve the requested properties for special choices of the functions

H, S_2, S_3. The subscript D stands for Dynamical, to distinguish the present field from the Stationary one $\mathbf{B}_S$ that will be introduced later on.

Regarding the electric field, it is enough to take the curl of $\mathbf{B}_D$ and integrate with respect to time (see (1)). This yields

$$\mathbf{E}_D = (E_r, E_\theta, E_\phi) = \frac{1}{\omega}\left(\frac{H}{r}\sqrt{1-x^2}\left[S_3' - \frac{x}{1-x^2}S_3 + \frac{m}{1-x^2}S_2\right]\cos\zeta,\ \left(H' + \frac{H}{r}\right)S_3\cos\zeta, \left(H' + \frac{H}{r}\right)S_2\sin\zeta\right), \tag{7}$$

where S_3 is differentiated with respect to x and H with respect to r. An equivalent version of (7) is found in (21). By direct calculation, it is possible to check that $\rho_D = \mathrm{div}\mathbf{E}_D = 0$ and that the electric field satisfies the vector wave equation. It is interesting to point out that in general $\mathbf{E}_D \cdot \mathbf{B}_D \neq 0$, providing an example of solutions of Maxwell's equations in vacuum where electric and magnetic fields are not orthogonal. Note that, at the radial points where $H = 0$, we obtain that $\mathbf{B}_D = 0$ and that $\mathbf{E}_D$ is tangential to the ball. Indeed, when $H = 0$, all the components of $\mathbf{B}_D$ in (6) are zero, whereas $\mathbf{E}_D$ in (7) has only the radial component E_r equal to zero.

The kind of rotating waves we are examining here may be straightforwardly related to the family of Vector Spherical Harmonics. Alternative solutions, naturally embedded in toroid shaped regions, are proposed in Chinosi et al[3] and Funaro.[4]

We can define the standard electromagnetic potentials by setting $\Phi_D = 0$ and recovering $\mathbf{A}_D$ through the integration of $\mathbf{E}_D$ in time. Since $\mathrm{div}\mathbf{A}_D = 0$, one discovers that we are in the Lorenz's gauge.

We conclude this section by defining the velocity vector field (also expressed in spherical coordinates):

$$\mathbf{V} = (V_r, V_\theta, V_\phi) = \left(0, 0, \frac{c\omega}{m} r\sin\theta\right), \tag{8}$$

which actually simulates the uniform rotation of our ball around the vertical axis. An important relation that will be used later on is the following one (see Section 3 for the proof):

$$\mathbf{E}_D + \mathbf{V}\times\mathbf{B}_D = -\nabla p_D \quad \text{with} \quad p_D = -\frac{1}{m\omega}(rH' + H)S_2\sin\theta\cos\zeta. \tag{9}$$

This says that the Lorentz's force, up to dimensional constant, is the gradient of a potential p_D. Note that this property does not hold in general for other choices of $\mathbf{V}$. Hence, Equation (9) is far from being trivial. Another solution, with the same properties of the one just examined is found in Funaro,[5] p. 147. Let us observe that in the homogeneous Maxwell's equations the role of $\mathbf{E}_D$ and $\mathbf{B}_D$ can be switched. With this we mean that, by the replacements $\mathbf{E}_D \to c\mathbf{B}_D$ and $c\mathbf{B}_D \to -\mathbf{E}_D$, we still obtain solutions. The property comes from direct substitution into Equations (1) and (2). This is not true anymore if we want to preserve the additional property (9).

3 | EXPLICIT COMPUTATION

We would like to impose that $\mathbf{B}_D$, as defined in (6), has zero divergence and satisfies the vector wave equation (5). More exactly, we require that

$$\frac{\partial^2\mathbf{B}_D}{\partial t^2} = -c^2\omega^2\mathbf{B}_D, \qquad \Delta\mathbf{B}_D = -\omega^2\mathbf{B}_D. \tag{10}$$

The symbol Δ denotes the vector Laplacian in spherical coordinates. We recall that S_2 and S_3 are functions of $x = \cos\theta$.

We find out that H has to satisfy the eigenvalue problem:

$$H'' + \frac{2H'}{r} - \ell(\ell+1)\frac{H}{r^2} = -\omega^2 H, \tag{11}$$

where the prime denotes the derivative with respect to r. The above equation is satisfied by spherical Bessel's functions.

Concerning the variable θ, the situation brings us to the so-called associated Legendre polynomials (see, e.g., Abramowitz and Stegun[1] p. 331) that satisfy the eingenvalue problem:

$$(1-x^2)S'' - 2xS' - \frac{m^2}{1-x^2}S = -\lambda S, \tag{12}$$

where now the prime denotes the derivative with respect to x. The values of λ correspond to numbers of the form $\ell(\ell+1)$, where ℓ is integer with $\ell \geq m$. In our case, S_2 and S_3 are related to S by the formulas:

$$S_2 = \frac{S}{\sqrt{1-x^2}}, \qquad S_3 = -\frac{S'}{m}\sqrt{1-x^2}. \tag{13}$$

The distribution of the fields $\mathbf{B}_D$ and $\mathbf{E}_D$ is rather complicated. It is relatively easy to display what happens on the surface of a ball having the radius $r = \hat{r}$ corresponding to a zero of H (recall that H is related to Bessel's functions, so that it displays infinite zeros). Indeed, for $H(\hat{r}) = 0$, by examining (6) and (7), we realize that $\mathbf{B}_D$ is identically zero on the surface, whereas $\mathbf{E}_D$ turns out to be tangential and organized to form several vortexes. The number of vortexes along the azimuthal direction is ruled by the parameter m. The number of vortexes spanned by the altitude angle depends on ℓ. A typical configuration is displayed in Figure 2. The displacement rotates about the vertical axis, as prescribed by the velocity field $\mathbf{V}$.

We briefly discuss the explicit solution for $m = \ell \geq 1$. This is given by setting:

$$S_2(\cos\theta) = (\sin\theta)^{m-1}, \qquad S_3(\cos\theta) = \cos\theta(\sin\theta)^{m-1}. \tag{14}$$

With the help of (14), we can better examine the distribution of the fields in the case $m = \ell = 2$. For $H \neq 0$, we get from (6):

$$\mathbf{B}_D = \frac{H(r)}{c}\,(0,\, \sin\theta\cos\zeta,\, \sin\theta\cos\theta\sin\zeta)\,. \tag{15}$$

For $H = 0$, we get instead from (7):

$$\mathbf{E}_D = \frac{H'(r)}{\omega}\,(0,\, \sin\theta\cos\theta\cos\zeta,\, \sin\theta\sin\zeta)\,. \tag{16}$$

The corresponding electric and magnetic fields are, respectively, shown in Figure 3.

As a final exercise, we check (9). We start by writing

$$\mathbf{V}\times\mathbf{B}_D = -\frac{\omega}{m}\,(HrS_2\sin\theta\cos\zeta,\, 0,\, 0)\,. \tag{17}$$

We have to prove that

$$-\nabla p_D = -\left(\frac{\partial p_D}{\partial r},\, \frac{1}{r}\frac{\partial p_D}{\partial\theta},\, \frac{1}{r\sin\theta}\frac{\partial p_D}{\partial\phi}\right) = \left((\mathbf{E}_D + \mathbf{V}\times\mathbf{B}_D)_r, E_\theta, E_\phi\right). \tag{18}$$

The verification is straightforward for the second and the third components. Concerning the first one, we begin by noting that

$$\ell(\ell+1)S_2 = -(1-x^2)S_2'' + 4xS_2' + \frac{m^2-1}{1-x^2}S_2 + 2S_2 = m\left[S_3' - \frac{x}{1-x^2}S_3 + \frac{m}{1-x^2}S_2\right], \tag{19}$$

where we used (12) and (13). The last term above is equal to the one in square brackets in (7). We finally have

$$\begin{aligned} -\frac{\partial p_D}{\partial r} &= \frac{1}{m\omega}(rH'' + 2H')S_2\sin\theta\cos\zeta = \frac{H}{m\omega}\left(\frac{1}{r}\ell(\ell+1) - \omega^2 r\right)S_2\sin\theta\cos\zeta \\ &= \frac{H}{m\omega r}\ell(\ell+1)S_2\sin\theta\cos\zeta + (\mathbf{V}\times\mathbf{B}_D)_r = (\mathbf{E}_D + \mathbf{V}\times\mathbf{B}_D)_r, \end{aligned} \tag{20}$$

where we used (11). This completes the proof of (18).

Note that, by virtue of (19), we can rewrite (7) as follows:

$$\mathbf{E}_D = \frac{1}{\omega}\left(\frac{H}{rm}\ell(\ell+1)S_2\sin\theta\cos\zeta, \left(H' + \frac{H}{r}\right)S_3\cos\zeta, \left(H' + \frac{H}{r}\right)S_2\sin\zeta\right). \tag{21}$$

4 | EXTENSION OUTSIDE THE BALL

We continue our exploration on the solutions (6) and (7) in the special case where $m = \ell$. We examine what happens outside the sphere. The expressions in (14) tell us that, for large m, the function S_2 assumes the value 1 for $\theta = \pi/2$ and goes fast to zero as approaching $\theta = 0$ or $\theta = \pi$. The fields are then concentrated in a flat annular region around the equator. As reported in Figure 3, for $H = 0$, the electric field is lined up with the equator and oscillates according to the rule: $\cos\zeta = \cos(c\omega t - m\phi)$. For $H \neq 0$, the magnetic field follows the same behavior, but it is oriented as the meridians. Based on (8), at a radius r, the intensity of the peripheral velocity of this equatorial wave is $V(r) = c\omega r/m$.

As r reaches a zero of H, the magnetic field vanishes. We believe that in this circumstance, there is a change of regime. In fact, it is difficult to accept the idea that, by increasing r, the quantity $V(r)$ is allowed to assume any possible value, as it would be for a rotating rigid body in classical mechanics. As specified in the introduction, we are examining a situation where, due to the special type of boundary constraints, there is no radial information escaping from the sphere. Thus, the case has to be handled differently from the lighthouse paradox. It is reasonable to guess instead that $V(r)$ does not exceed too much the speed of light in vacuum. This is thinkable if we suppose that the process happens through some quantized steps. Indeed, it is possible to build encapsulated shells. Inside each one of them, we are solving a wave type equation. The angular velocity decreases by passing from a shell to an external one. Moreover, such a passage can be made in continuous way. We show how this extraordinary fact can be achieved.

We adapt to the present circumstances a situation already studied in Funaro.[6] The aim is to construct solutions defined on a circular crown, in such a way that the velocity at the internal boundary is more or less the same (in magnitude) than that at the external boundary. This construction relies on the possibility to find eigenfunctions of the Laplace operator, corresponding to eigenvalues of multiplicity four, at least. Technically, the question is reduced to find suitable periodic solutions of the wave equations (5). After separation of variables and further simplifications ($m = \ell$), the problem can be studied for a scalar equation in two dimensions, although the general discussion in 3D involves the same ingredients. The domain is an annular region between the radii $r_{\min}$ and $r_{\max}$. Homogeneous Dirichlet boundary conditions are assumed, though such a constraint is not strict. The solution must develop in such a way that, in proximity of the inner boundary, the shift is governed by the rule $\cos(c\omega t - m_A\phi)$, where m_A is an integer. At the external boundary we should have instead $\cos(c\omega t - m_B\phi)$, where $|m_B| > |m_A|$ is another integer. At these boundaries, the velocity of rotation is expressed by (8). If the rotating body was rigid, the external velocity would be larger than the internal one, directly depending on the ratio $r_{\max}/r_{\min}$. Here, we can play instead with the values of the integers m_A and m_B, in order to obtain that the intensity of the inner velocity $c\omega r_{\min}/m_A$ is comparable with the external one $c\omega r_{\max}/m_B$.

Such an analysis is not trivial and passes through the determination of the zeros of the Laplacian eigenfunctions in the domain. In fact, not all the configurations are possible. The parameters to play with are m_A, m_B, ω, and $r_{\max}/r_{\min}$. They have to be detected in order to have a basis of at least four orthogonal eigenfunctions corresponding to the same eigenvalue (which, as a consequence, must have multiplicity equal to 4). Interesting dynamical patterns are then obtained from suitable linear combinations of these eigenfunctions.

The underlying idea of this construction is to recreate something similar to an interconnected set of gears of different size: the small one turning fast imparts a slow rotation to the big one. The case of an annular region is better described by a ball-bearing assembly (see Figure 4), where, in smooth way, the momentum of the internal support is transferred to the external one, avoiding the inconveniences (and the paradoxes) related to the rotation of a rigid body.

From the practical viewpoint, let $r_{\min}$ denote the interior radius of the annulus. We define the following function:

$$F_m(r) = \frac{1}{\sqrt{\omega r}}\left(Y_{m+\frac{1}{2}}(\omega r_{\min})J_{m+\frac{1}{2}}(\omega r) - J_{m+\frac{1}{2}}(\omega r_{\min})Y_{m+\frac{1}{2}}(\omega r)\right), \tag{22}$$

where, for a given α, J_α and Y_α are the Bessel's functions of the first and the second kind, respectively. It is easy to check that $F_m(r_{\min}) = 0$.

We would like now to find two different integers m_A and m_B, a value of the parameter ω, and a radius $r_{\max}$ of the external circumference of the annulus. This has to be done in order to satisfy the conditions:

$$F_{m_A}(r_{\max}) = 0, \qquad F_{m_B}(r_{\max}) = 0. \tag{23}$$

The explanation is as follows. We require homogeneous Dirichlet conditions on the boundaries of the annulus (internal and external), and we want this to be simultaneously achieved for different frequencies m_A and m_B. Such a problem does not always admit solution. Possible allowed combinations (among infinite others) for $r_{\min} = 1$ are $m_A = 2, m_B = 5, \omega \approx 1.97, r_{\max} \approx 4.75$; $m_A = 2, m_B = 6, \omega \approx 3.72, r_{\max} \approx 2.83$; or $m_A = 2, m_B = 8, \omega \approx 2.39, r_{\max} \approx 5.35$. The last case is represented in Figure 5.

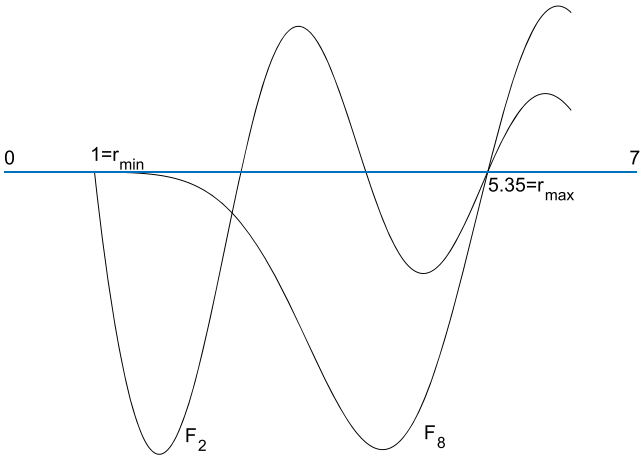

FIGURE 5 Both the two functions F_2 and F_8 vanish at $r_{\min} = 1$ and $r_{\max} \approx 5.35$. The amplitude of the functions have been suitably rescaled to make more clear the graphical output [Colour figure can be viewed at wileyonlinelibrary.com]

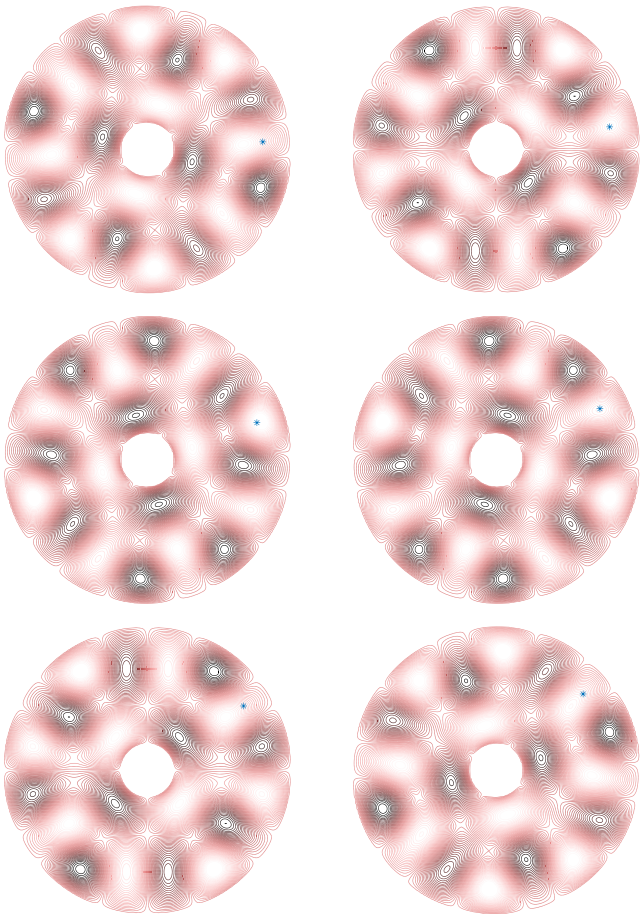

FIGURE 6 Solution of the wave equation for a period of time. As the central core makes a half clockwise rotation, the peripheral part accomplishes an eighth of a cycle in anticlockwise manner, as testified by the position of the asterisk [Colour figure can be viewed at wileyonlinelibrary.com]

Reminding once again that we are examining the case $m = \ell$ (see also (14)), the expression in (22) has a link with the eigenfunctions studied so far, where the dependence from the variable θ is neglected. We can actually define

$$\Phi_m(r,\phi) = \alpha_m F_m(r)\cos(m\phi), \qquad \Psi_m(r,\phi) = \beta_m F_m(r)\sin(m\phi), \tag{24}$$

for arbitrary multiplicative constants α_m and β_m. By restoring the part in the variable θ, these are indeed two orthogonal eigenfunctions with eigenvalue $-\omega^2$. We get solutions of the wave equation by introducing combinations depending on time. For different values of m_A and m_B, we can write

$$\Phi_{m_A}\sin(c\omega t) + \Phi_{m_B}\cos(c\omega t) + \Psi_{m_A}\sin(c\omega(t+t_0)) + \Psi_{m_B}\cos(c\omega(t+t_0)), \tag{25}$$

where t_0 is a time shift.

By suitably adjusting t_0, α_m, and β_m, we get interesting evolution patterns. This is the case for instance of the plots of Figure 6, where $m_A = 2$, $m_B = 8$, $\omega \approx 2.39$, and $r_{\max}/r_{\min} = 5.35$. The combination of Φ_2 and Ψ_2 gives origin to the part of the solution that rotates with azimuth $\zeta = c\omega t - 2\phi$ and internal velocity $c\omega r_{\min}/2 \approx 1.2c$. Similarly, the part related to Φ_8 and Ψ_8 counter rotates with azimuth $\zeta = c\omega t + 8\phi$ and external velocity $c\omega r_{\max}/8 \approx 1.6c$. Note that if the body was rigid, the external velocity would have been approximately equal to $6.4c$, exaggeratedly exceeding the speed of light (see the comments of Section 6). Another example of this type is shown in Figure 4, where the parameters are $m_A = 4$, $m_B = 20$, $\omega \approx 13$, and $r_{\max}/r_{\min} \approx 2$. Here, the external velocity is even lower than the internal one. These plots can be however fully understood and appreciated only with the help of animations.

5 | VALIDITY IN A MORE EXTENDED CONTEXT

Going back to Section 1, we can get new solutions by adding suitable stationary (not depending on time) fields $\mathbf{E}_S$ and $\mathbf{B}_S$. This can be easily done if we assume that $\rho_S = \mathrm{div}\mathbf{E}_S$ is constant (in particular we may choose $\rho_S = q$, for a given q). Thus, we set: $\mathbf{E} = \mathbf{E}_D + \mathbf{E}_S$, $\mathbf{B} = \mathbf{B}_D + \mathbf{B}_S$, $\rho = \rho_D + \rho_S = \rho_S = q$, $p = p_D + p_S$. In addition, we take $\mathbf{V}$ as in (8), and we replace (1) by the Ampère's law with a source term:

$$\frac{\partial \mathbf{E}}{\partial t} = c^2\mathrm{curl}\mathbf{B} - \rho\mathbf{V}. \tag{26}$$

By plugging the new fields in (2), (3), and (26), we must have

$$c^2\mathrm{curl}\mathbf{B}_S = \rho_S\mathbf{V}, \tag{27}$$

$$\mathrm{curl}\mathbf{E}_S = (0,0,0), \tag{28}$$

$$\mathrm{div}\mathbf{B}_S = 0. \tag{29}$$

A possible choice for the stationary fields is

$$\mathbf{E}_S = \frac{q}{3}(r,0,0) = \frac{q}{6}\nabla r^2, \qquad \mathbf{B}_S = \frac{q\omega}{5mc}\left(-r^2\cos\theta, 2r^2\sin\theta, 0\right). \tag{30}$$

Let us observe that the magnetic field written above is exactly the one generated by a rotating ball, uniformly charged (see, e.g., Griffiths,[7] example 5.11). We also get

$$\mathbf{V}\times\mathbf{B}_S = -\frac{q\omega^2}{5m^2}\left(2r^3\sin^2\theta, r^3\sin\theta\cos\theta, 0\right) = -\frac{q\omega^2}{10m^2}\nabla(r^4\sin^2\theta). \tag{31}$$

From (30) and the above relation, we discover that Equation (9) is also satisfied by the combined fields $\mathbf{E} = \mathbf{E}_D + \mathbf{E}_S$ and $\mathbf{B} = \mathbf{B}_D + \mathbf{B}_S$. Other (singular) stationary fields compatible with the set of equations are the following ones (up to multiplicative constants):

$$\mathbf{E}_S = \left(\frac{1}{r^2}, 0, 0\right), \qquad \mathbf{B}_S = \left(\frac{2\cos\theta}{r^3}, \frac{\sin\theta}{r^3}, 0\right). \tag{32}$$

In this case, we get $\text{div}\mathbf{B} = 0$, $\text{curl}\mathbf{B} = 0$, $\mathbf{V} \times \mathbf{B} = (c\omega/m)\nabla(r^{-1}\sin^2\theta)$ and $\rho_S = 0$. At this point, connections with standard MHD can also be established. For example, we get the induction equation:

$$\begin{aligned}\frac{\partial \mathbf{B}}{\partial t} &= \frac{\partial}{\partial t}(\mathbf{B}_D + \mathbf{B}_S) = \frac{\partial \mathbf{B}_D}{\partial t} = -\text{curl}\mathbf{E}_D \\ &= \text{curl}(\mathbf{V} \times \mathbf{B}_D) = \text{curl}[\mathbf{V} \times (\mathbf{B}_D + \mathbf{B}_S)] = \text{curl}(\mathbf{V} \times \mathbf{B}),\end{aligned} \tag{33}$$

where, in the order, we used that $\mathbf{B}_S$ is stationary and then (2), (9), and (31). The literature on exact solutions in MHD is quite rich. We just mention a few references.[8–10] The results of this section add further knowledge.

6 | RELATIONSHIPS WITH GENERAL RELATIVITY

In the introduction, we specified that the aspects related to the theory of relativity were out of the scope of this paper. We add however some observations. At the end of Section 4, we claimed that our rotating waves, even if they solve the full set of Maxwell's equations in vacuum, display regions where the information evolves at speeds different from that of light. The anomaly could be explained by introducing some corrective terms due to relativity. By the way, we do not think that Special Relativity would be a sufficient tool for investigating this aspect. As a matter of fact, the complicated dynamics of the EM environment surrounding the rotating ball, being a form of energy, is certainly connected to a global deformation of the space-time. An explicit knowledge of this modification is usually recovered from the solution of Einstein's equation, by plugging on the right-hand side the EM stress tensor. This accomplishment is far from being trivial. Earlier results for plane waves were proposed in.[11] Numerous exact solutions can be found in[5] and.[12] The EM evolution follows the geodesics of a geometry which is itself a consequence of the movement. Formally, a density of mass can be assigned to the metric (usually, one examines the term g_{00} of the tensor). This does not mean that there are real masses (except for the tiny particles of the plasma, whose contribution is negligible). Light does not rotate as a consequence of huge central masses deforming the space-time. Nevertheless, we may assume the existence of a continuum of distributed density of "mass," after giving to this term a sort of extended meaning. The forces in action are dynamically changing and may attain zero average in portions of space, when observed in a period of time. Even if it is not directly detectable, this form of energy can have significant intensities that are spread on entire volumes. The general treatment in the gravitational framework suggests to suitably combine the EM stress tensor with a mass tensor (see Shibata and Sekiguchi[13]), so that to appreciate the interactions of all the possible forces. Evidently, the numerical solution of these problems is rather challenging. The vast literature on the study and the numerical approximation of binary black holes space-time (some sample papers are[14–19]) may help devising similar computational techniques for the solution of these nasty equations within the EM context.

7 | HINTS ON THE CONSTITUTION OF THE HELIOSPHERE

Since the pioneering papers of H. Alfvén,[20] the study of the evolving plasma in the Heliosphere is a widely investigated subject. Moreover, the role of plasma is recognized to be a primary factor to understand our universe at all scales of magnitude (see, e.g., Peratt[21,22]). The EM environment introduced in the previous sections may represent a possible background distribution, in support of more complex phenomena. From the results so far discussed, we advance some conjectures about our Sun. We refer to the circular electric patterns of Figure 2. Assuming that the solar cells have an averaged diameter $d = 1100$ km, there are about $2\pi R_\odot/d \approx 4000$ of them along the equatorial circumference ($R_\odot$ being the Sun radius). This means that $m \approx 2000$. We can choose ℓ in such a way that $\ell/m \approx 2$. With this choice, the number of cells lined up along the equator is approximately equal to those lined up along a meridian. Roughly, the Bessel's function $J_\alpha(r)$ has its first positive root for $r \approx \alpha$. The function is practically zero, presenting a sudden bump just before such a root (see for instance the plot of Figure 7, representing the function J_{50}). This says that the cells have a relatively small depth. In the case of $J_{\ell+1/2}(\omega r)$, we then get $\omega \approx \ell/R_\odot$. According to (8), the intensity of $\mathbf{V}$ on the equator is $|\mathbf{V}| = c\omega R_\odot/m \approx c\ell/m \approx 2c$. Therefore, this final result is almost independent of all the parameters, with the exception of c. We recall that c appears in the wave equations (5).

The solar body is a medium containing material particles, whose movement is accompanied by their EM interactions. Particles supply the EM field in their motion and, at the same time, they are dragged by a mechanism related to Lorentz's force. Due to the fact that they are massive, the velocity constant c should be suitably reduced, by arguing that the medium

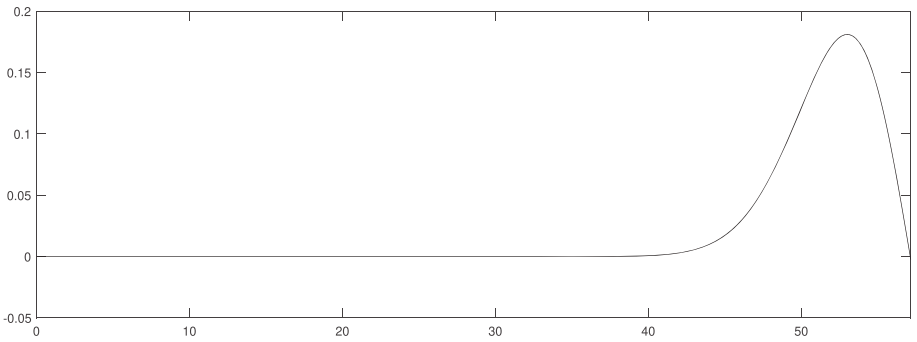

FIGURE 7 Plot of the Bessel function J_{50}

intrinsically presents a relative dielectric constant higher than that of vacuum, forcing the information described by $\mathbf{V}$ to evolve at lower velocities. A quantitative analysis (too technical for the purpose of this paper) involves the knowledge of the electrical conductivity σ of the Sun (see, e.g., Stix,[23] section 8.1.2). If c is the speed of light in vacuum, a period of rotation around the vertical axis, turns out to be approximately 4.65 seconds. This is 16×10^3 times smaller than the revolution period of the Sun of about 27 days. Thus, c must be reduced accordingly.

We can provide an alternative explanation. Instead of adapting the value of c to the conductive characteristics of the solar plasma, we can continue to suppose that c is the speed of light in vacuum. Therefore, there is a high-frequency pure EM wave turning around that acts as a forcing term. Such a wave may be rather simple as in Figure 3. As charged particles are present, they are dragged into a rotatory motion, but they do this by following patterns that are strictly related to various physical quantities, such as the intensity of the charges involved, their masses, their density within the plasma. The slower global motion is a consequence of the above restrictions, whereas the EM information still develops at its classical speed. This viewpoint stimulates a further conjecture. A star is formed when, due to the creation of a swirl in the EM background (like a tornado in air), preexisting particles glue together (by electrodynamical and gravitational forces) conferring stability to the newborn structure and finding a state of dynamical equilibrium. We also observe that vortexes of electric type on the solar surface may give raise to magnetic loops (spicules), as a trivial consequence of Faraday's law. These filaments, that can carry particles as well, ignite the mechanism at the origin of solar flares. Of course, our construction is elementary if compared to the complexity of a star. On the other hand, we are just building our assumptions based on the solutions of simplified models.

Outside the massive bulk of the star, we still have plasma, but with an extremely small concentration of particles. We are basically in vacuum so that the information now really evolves at speeds comparable to that of light. By this, we do not mean that particles necessarily travel fast. We argue that what develops at luminous velocities is the flow of EM information in which they are embedded in. The Sun has several ways to let us know its presence. First, it emits photons. These tiny energy packets escape as a consequence of chemical or subatomic reactions. Photons constitute the visible part, since they can be detected with our eyes or instruments. The EM activity at the exterior of the Sun can be enriched by the addition of pseudo-stationary components simulating the so-called solar wind. Here, the line of force corotate with the Sun (see Figure 1, left), and may be either closed or open loops depending on the distance (see Ferraro and Bhatia[24] and Pneuman and Kopp[25]). To this extent, we characterize the idea of Parker's spiral (see Parker[26]), as a further message imprinted on the plasma. Exact solutions of this type, in the context of MHD, are given for instance in Asghar et al.[27] Analytic solutions for the spiraling fields generated by a rotating magnetic dipole are given in Sarychev.[28]

8 | SPECULATIONS ABOUT THE TITIUS–BODE LAW

We claim that there is another mean, only indirectly observable, used by the Sun to leave fingerprints on the surrounding space. The turbulent EM status of the star induces the creation of complicated (but well organized) whirls and spirals as described in this paper. The Solar corona should correspond to the first layer, although its dynamics is governed by the nonlinear equations of MHD, thus is far more complex than what illustrated here. This process may however generate a sequence of encapsulated shells, whose size reasonably grows geometrically. Inside each shell, there are trapped EM waves, coordinately traveling and performing a peculiar dance. The transition between a shell and the next one happens with continuity. Differently from Colburn and Sonett,[29] we have shown here that it is possible to connect the different domains by avoiding shocks on the magnetic fields. We also assumed that the interfaces are surfaces displaying zero magnetic field, though this hypothesis may be reviewed at the occurrence. These systems evolve at an averaged speed

comparable to that of light. As they become larger, the angular velocity diminishes. We also observe that rotating EM solutions constrained in finite regions of space are well suited for domains having annular topology.[3,4,6] This may suggest developments based on other geometries. In reality, changes in the magnetic field have been detected by interplanetary probes. Some theories have been consequently developed (see previous studies[30–32]). Quick intermittent magnetic reversals in proximity of the Sun have been also reported (see, for instance, previous studies[33–35]).

According to our viewpoint, there may be in the Heliosphere an organized set of shells which is not directly visible. We can however appreciate its existence in indirect way. Perhaps, this construction may contribute to explain the formation of planets, initially in a state of fragments (planetesimals) and successively compacted by self-gravity and the action of an organized plasma (see, e.g., Alfvén[20,36]). An EM prearranged environment may force the selection of distant regions of space where bunches of massive objects may meet and join together. The analysis of the first modes involved in the construction of the external shells (consider the case $m = \ell$ examined in Section 5) says that a privileged direction is that of the equatorial plane. This suggests a possible explanation of the (almost) coplanar distribution of the planets. Moreover, it seems that there are more chances to find matter in zones where the interface magnetic field vanishes. Indeed, according to Karsten and Pogosian,[37] charged particles actually tend to accumulate in regions where the magnetic field is of weakest strength.

Due to the geometrical growth of the shells, we can advocate for the existence of specific spots where it is more likely to find planets. This turns out to be in agreement with the Titius–Bode law, in which the averaged distance of the planets from the Sun follows approximately a geometric growth rate: $0.4 + 0.3 \times 2^k$, where the unity of measure of the distance is expressed in Astronomic Units. Note that in the right picture of Figure 4, the ratio $r_{\max}/r_{\min}$ is actually very close to 2. It is worth to be noted that Neptune's orbit does not comply with the law, since we should approximately have $k = 6.6$ ($k = 6$ Uranus, $k = 7$ Pluto). On the other hand, the magnetic field of Neptune is known to be rather anomalous (longitudinal instead of transversal). Astonishingly, this is in agreement with our viewpoint. Indeed, the planet seems to be trapped in the middle of a shell rather than at the transition zone between two shells.

The Titius–Bode law is an intriguing subject still lacking of a convincing explanation. Some related publications are for instance.[38–42] Although its mechanism is not clearly understood, the law is currently applied in the search of the so-called exoplanets. Our hope is that the arguments put forth in the present paper may contribute to a better comprehension of this phenomenon.

ACKNOWLEDGEMENT

There are no funders to report for this submission. Open Access Funding provided by Universita degli Studi di Camerino within the CRUI-CARE Agreement.

CONFLICT OF INTEREST

The authors declare no conflict of interest.

ORCID

Lorella Fatone https://orcid.org/0000-0001-7163-5490

REFERENCES

1. Abramowitz M, Stegun IA, eds. *Handbook of Mathematical Functions with Formulas, Graphs and Mathematical Tables*, Applied Mathematics Series, vol. 55: Dover Publications; 1965.
2. Landau LD, Lifschits EM. *The Classical Theory of Fields*. 3rd ed. Pergamon Press; 1971.
3. Chinosi C, Della Croce L, Funaro D. Rotating electromagnetic waves in toroid-shaped regions. *Int J Modern Phys C*. 2010;21(1):11-32.
4. Funaro D. Electromagnetic waves in annular regions. *Appl Sci MDPI*. 2020;10(5):1780.
5. Funaro D. *Electromagnetism and the Structure of Matter*. World Scientific; 2008.
6. Funaro D. Trapping electromagnetic solitons in cylinders. *Math Model Anal*. 2014;19(1):44-51.
7. Griffiths DJ. *Introduction to Electrodynamics*. 3rd ed. Prentice Hall; 2007.
8. Golovin SV, Dudnik MN. Unsteady flows with a constant total pressure described by the equations of ideal magnetohydrodynamics. *J Appl Mech Tech Phys*. 2014;55(2):234-246.
9. Picard PY. Some exact solutions of the ideal MHD equations through symmetry reduction method. *J Math Anal Appl*. 2008;337:360-385.
10. Shokri M, Sadooghi N. Novel self-similar rotating solutions of non-ideal transverse magnetohydrodynamics. *Phys Rev D*. 2017;96:116008.
11. Bondi H, Pirani FAE, Robinson I. Gravitational waves in general relativity, III, exact plane waves. *Proc R Soc Lond A*. 1959;251:519-533.

12. Funaro D. *From Photons to Atoms: the Electromagnetic Nature of Matter*. World Scientific; 2019.
13. Shibata M, Sekiguchi Y-I. Magnetohydrodynamics in full general relativity: formulation and tests. *Phys Rev D*. 2005;72:044014.
14. Blanchet L. Gravitational radiation from post-Newtonian sources and inspiralling compact binaries. *Living Rev Relativ*. 2002;5:3.
15. Price RH, Pullin J. Colliding black holes: the close limit. *Phys Rev Lett*. 1994;72:3297.
16. Brandt S, Correll R, Gomez R, et al. Grazing collisions of black holes via the excision of singularities. *Phys Rev Lett*. 2000;85:5496.
17. Brügmann B. Binary black hole mergers in 3D numerical relativity. *Int J Mod Phys*. 1999;D8:85.
18. Lau SR. Implicit-explicit (IMEX) evolution of single black holes. *Phys Rev D*. 2011;95:084023.
19. Pretorius F. Evolution of binary black hole spacetimes. *Phys Rev Lett*. 2005;95:121101.
20. Alfvén H. *On the Origin of the Solar System*. 1st ed. Clarendon Press; 1954.
21. Peratt AL. Plasma cosmology. *Sky & Telescope*. 1992:136.
22. Peratt AL. *Physics of the Plasma Universe*. 2nd ed. Springer; 2015.
23. Stix M. *The Sun, An Introduction*. Springer; 1989.
24. Ferraro VCA, Bhatia VB. Corotation and solar wind in the solar corona and interplanetary medium. *Astrophys J*. 1967;147:220-229.
25. Pneuman GW, Kopp RA. Gas-magnetic field interactions in the solar corona. *Solar Phys*. 1971;18:258-270.
26. Parker EN. Dynamics of the interplanetary gas and magnetic fields. *Astrophys J*. 1958;128:664.
27. Asghar S, Khan M, Siddiqui AM, Hayat T. Exact solutions for magnetohydrodynamic flow in a rotating fluid. *Acta Mech Sinica*. 2002;18(3):244-251.
28. Sarychev V. Electromagnetic field of a rotating magnetic dipole and electric-charge motion in this field. *Radiophysics Quantum Electron*. 2009;52(12):900-907.
29. Colburn DS, Sonett CP. Discontinuities in the solar wind. *Space Sci Rev*. 1966;5:439-506.
30. Burlaga LF. Directional discontinuities in the interplanetary magnetic field. *Solar Phys*. 1969;7:54-71.
31. Burlaga LF, Ness NF, Berdichevsky DB, et al. Magnetic field and particle measurements made by Voyager 2 at and near the heliopause. *Nature Astron*. 2019;3:1007-1012.
32. Siscoe GL, Davis LJr., Coleman PJJr., Smith EJ, Jones DE. Power spectra and discontinuities of the interplanetary magnetic field: Mariner 4. *J Geophysical Res*. 1968;73(1):61-82.
33. Bale SD, Badman ST, Bonnell JW, et al. Highly structured slow solar wind emerging from an equatorial coronal hole. *Nature*. 2019;576:237-242.
34. Horbury TS, Matteini L, Stansby D. Short, large-amplitude speed enhancements in the near-Sunfast solar wind. *Mon Not R Astron Soc*. 2018;478:1980-1986.
35. Kasper JC, Bale SD, Belcher JW, et al. Alfvénic velocity spikes and rotational flows in the near-Sun solar wind. *Nature*. 2019;576:228-231.
36. Alfvén H. Cosmology in the plasma universe: an introductory exposition. *IEEE Trans Plasma Sci*. 1990;18:5-10.
37. Karsten J, Pogosian L. Relieving the Hubble tension with primordial magnetic fields. *Phys Rev Lett*. 2020;125:181302.
38. Hayes W, Tremaine S. Fitting selected random solar systems to Titius-Bode laws. *Icarus*. 1998;135:549-557.
39. Lynch P. On the significance of the Titius-Bode law for the distribution of the planets. *Mon Not R Astron Soc*. 2003;341(4):1174-1178.
40. Nieto M. *The Titius-Bode Law of Planetary Distances: Its History and Theory*. 1st ed. Pergamon Press; 1972.
41. Nottale L. *Fractal Space-Time and Microphysics: Towards a Theory of Scale Relativity*. World Scientific; 1993.
42. Nottale L, Schumacher G, Gay J. Scale relativity and quantization of the solar system. *Astron Astrophys*. 1997;322:1018-1025.

How to cite this article: Fatone L, Funaro D. Electromagnetic fields simulating a rotating sphere and its exterior with implications to the modeling of the heliosphere. *Math Meth Appl Sci*. 2023;46(2):1952-1963. doi:10.1002/mma.8621